Strongly correlated systems in atomic and condensed matter physics

Lecture notes

by Eugene Demler

ETH Zurich

December 6, 2023

Chapter 13

Pairing with spin imbalance

In the Chapter we discuss the situation when pairing arises on top of the spin imbalance

13.1 BCS pairing

We first discuss the possibility of conventional pairing of $k\uparrow$ and $-k\downarrow$ fermions. Mean-field Hamiltonian can be written as (see also Chapter 10)

$$\mathcal{H} = \sum_{k\sigma} (\xi_k \, - \, h\,\sigma \,) \, c^\dagger_{k\sigma} \, c_{k\sigma} + \sum_k (\, \Delta_k \, c^\dagger_{k\uparrow} \, c^\dagger_{-k\downarrow} \, - \, \Delta^*_k \, c_{-k\downarrow} \, c_{k\uparrow} - \Delta_k \, b^*_k \,) \quad (13.1)$$

Doing the same Bogoliubov diagonalization procedure as for the spin balanced case we obtain

$$\mathcal{H} = \sum_k \, (E_k - h) \, \gamma^\dagger_{k\uparrow} \, \gamma_{k\uparrow} + \sum_k \, (E_k + h) \, \gamma^\dagger_{k\downarrow} \, \gamma_{k\downarrow} \quad (13.2)$$

We can calculate free energy in the mean-field approximation

$$\begin{aligned} \Omega \;\; &= \;\; -\frac{|\Delta|^2}{V} + \int_k \frac{d^3k}{(2\pi)^3} \, (\xi_k - E_k) \\ &- \;\; \frac{1}{\beta} \int_k \frac{d^3k}{(2\pi)^3} \, [\, \log(1 + e^{-\beta(E_k - h)}) \, + \, \log(1 + e^{-\beta(E_k + h)}) \,] \end{aligned} \quad (13.3)$$

The first term corresponds to the state without quasiparticles, the second term to thermally excited quasiparticles. Equilibrium gap can be found by minimizing (13.3) with respect to Δ. We should also remember that V is the microscopic interaction that needs to be related to the scattering length by the usual relation

$$\frac{m}{4\pi a} = \frac{1}{V} + \int \frac{d^3k}{(2\pi)^3} \, \frac{1}{2\epsilon_k} \quad (13.4)$$

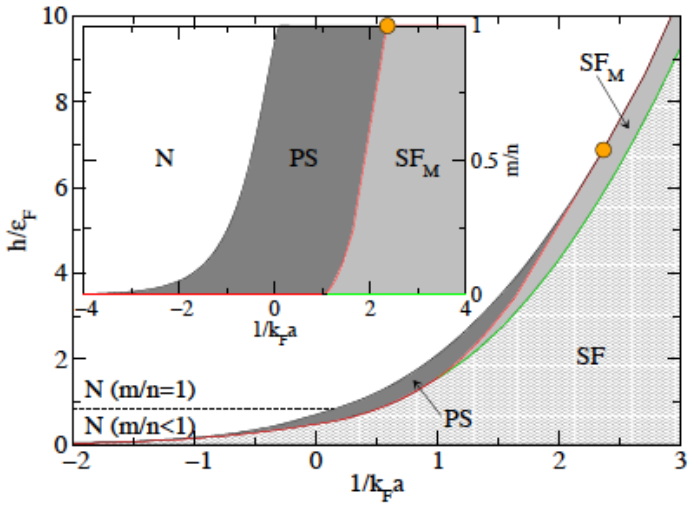

Figure 13.1: Phase diagram for the spin polarized BCS solution at $T = 0$. There are four different regions: the normal (N) state, the phase-separated (PS) state, spin unpolarized superfuid (SF), and the magnetized superfluid ($\mathrm{SF_M}$). Figure taken from [6].

Note that equation (13.3) recognizes when $E_k - h$ becomes negative and the quasiparticle state becomes occupied

$$-\frac{1}{\beta}\log(1+e^{-\beta(E_k-h)}) \;=\; E_k - h + \log(1+e^{-\beta(h-E_k)}) \tag{13.5}$$

In constructing this phase diagram it is not sufficient to optimize (13.3) with respect to Δ. One also needs to check that the system has positive compressibility with respect to spin imbalance. This means that the second derivative of the free energy with respect to h should be positive. When the second derivative is negative, a phase separated state is energetically favorable. To understand the nature of phase separated state one needs to do a Maxwell construction. Phase diagram based on (13.3) is shown in fig. 13.1. The main figure shows that the superfluid state is not affected by the Zeeman field until some finite value of h. Indeed at $T = 0$ there should be no effect of h when it is smaller than min E_k. Hence we have a state with strictly zero magnetization for a range of Zeeman fields. This is not surprising considering that the BCS state has a gap. In the $\mathrm{SF_M}$ we get superfluid state with finite polarization as a stable phase. Note that it only exists on the BEC side far enough from the resonance. It can be understood as a mixture of bosonic molecules and fermionic atoms. When repulsion between the two becomes too strong, the system becomes unstable. In the PS (phase separation) regime partially polarized state is thermodynamically unstable. The tricritical point is at $\frac{1}{k_F a} = 2.37$. Finite temperature phase diagram is shown in figure 13.2.

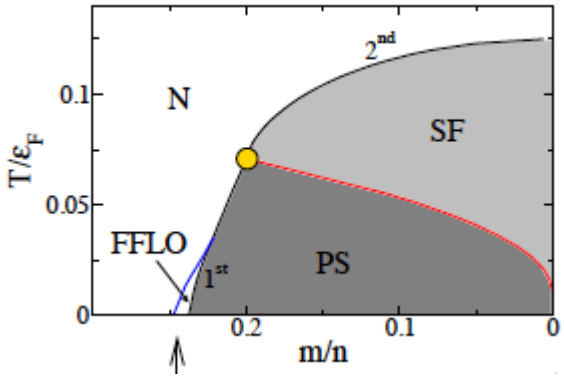

Figure 13.2: Phase diagram for the spin polarized BCS solution at finite temperature. Yellow dot denotes the tricritical point. Small region of the FFLO phase is discussed in section 13.2. Figure taken from [6].

13.2 FFLO phases

When Fermi surfaces are mismatched, it may become favorable to pair fermions at finite wavevector (see fig 13.3). Possibility of the FFLO phase has been a controversial subject in solid state systems during the last few decades (see [11] for a recent review). In electronic systems it is not easy to reach a regime where the Zeeman effect of the magnetic field dominates over the orbital part (it has been suggested that this may be possible in layered systems with magnetic field along the planes). Inhomogenous pairing and FFLO type phases are also an important subject for quark pairing in high density QCD [2].

To find the line where the normal state becomes unstable toward finite q pairing we consider Cooperon propagators at finite momenta and require their frequency to go to zero (see Chapter 12)

$$-\frac{m}{4\pi a} = \int \frac{d^3k}{(2\pi)^3} \left[\frac{1 - f(\xi_{k+q\uparrow}) - f(\xi_{-k\downarrow})}{\xi_{k+q\uparrow} + \xi_{-k\downarrow}} \right] \tag{13.6}$$

For given spin imbalance this equation needs to be optimized with respect to q, i.e. we need to find the first unstable mode. We need to compare this line to the $q = 0$ instability line discussed earlier. For a range of interaction strengths we find that we first get instability to an inhomogenous FFLO phase (see fig. 13.5).

It is difficult to perform detailed analysis of states with spatially varying $\Delta(r)$. Schematic argument shown in figure 13.3 suggests the wavevector of the ordered state but not its direction. The simplest possibility is to consider just one ordering wavevector. This is the state first proposed by Fulde and Ferrell[9]. In this case the amplitude of the order parameter is constant but the phase of the order parameter is winding uniformly in space. A better option is take $\pm q$ combination, i.e. an order paramater that changes as $\cos qz$. This possibility was

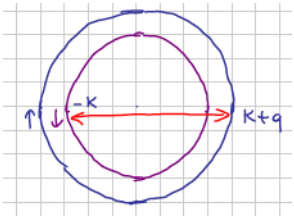

Figure 13.3: Mismatch of Fermi surfaces for systems with spin imbalance.

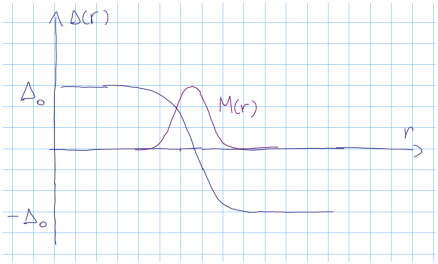

Figure 13.4: Schematic picture of the domain wall in the superconducting state. Order parameter changes. Region where the gap goes to zero allows low energy quasiparticles and can accomodate spin polarization.

considered by Larkin and Ovchinnikov[10]. More detailed calculations in n two and three dimensions require including several ordering directions[1]. Energy of the variational state is also very sensitive to including higher harmonics. On the other hand the system is also close to phase separation and small corrections to the energy can result is the wrong sign of compressibility. Hence the question of stability regime of the FLLO phase remains open.

One indication of the tendency toward inhomogeneous pairing state is a negative energy of the domain wall. Having a domain wall increases the pairing energy since it suppresses the pairing amplitude and forces the order parameter to be spatially modulated. However it allows finite magnetization to develop in the region where the gap goes to zero, which can lower the Zeeman energy (see fig. 13.6.) Figure 13.5 shows results of Bogoliubov de Gennes calculations for the domain wall energy (see section 13.5 for details). Negative energy of the domain walls however does not provide sufficient condition for the existence of the FFLO phase. One also needs to know interaction between domain walls. When interaction is repulsive, a crystal of domain walls will be created, which corresponds to the FFLO type phase. When interaction between domain walls is attractive, the system will phase separate.

One important exception is one dimensional systems. In this case exact Bethe ansatz solutions are available, whcih allows to establish rigorously the existence and domain of stability of the FFLO phase[12]. Figure 13.7 shows the phase diagram of a one dimensional Fermi mixture with imbalanced populations.

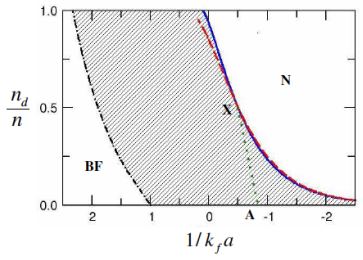

Figure 13.5: Phase diagram of fermionic paired systems with spin imbalance. Blue line shows instability line from the normal to the unform paired state. Dashed red line shows instability line from the normal to the pairing phase at finite momentum, the so-called FFLO phases. Dotted line XA shows where the domain wall energy becomes negative (to the right of this line). Hence one expects the appearance of the FFLO phase in the shaded area to the right of the XA line. Shaded region to the left of the XA line is phase separated. BF is a homogeneous superflid phase (Bose-Fermi mixture). Figure taken from [15].

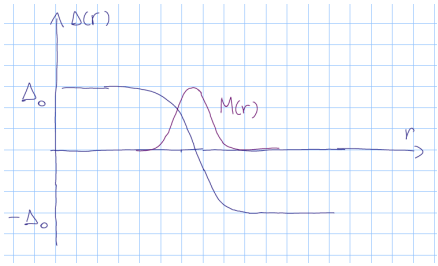

Figure 13.6: Schematic picture of the domain wall in the superconducting state. Order parameter changes. Region where the gap goes to zero allows low energy quasiparticles and can accomodate spin polarization.

13.3 Experimental studies of the FFLO phase

Experiments by the MIT group did not observe any indications of the FFLO phase in 3d traps[8] (see figs. 13.9, 13.10).

Indirect evidence of the FFLO type phases has been observed in one dimensional systems[7] (see fig. 13.11). In a parabolic trap the inhomogeneous potential can be thought of as making a cut through the phase diagram as shown in the figure 13.7. A surprising consequence of the phase diagram 13.7 is that for small polarizations one expects to find FFLO type states with partial polarization in the center of the trap (higher density regions) and fully paired states near the edges. This is the precise opposite of what one finds in 3d traps, where the center is fully paired and all polarization is expelled to the edges. Such reversal of the spatial distribution of polarization is a result of the special property of 1d systems: the density of states has a singularity at the bottom of the band. If we recall that in the usual BCS theory the effective coupling

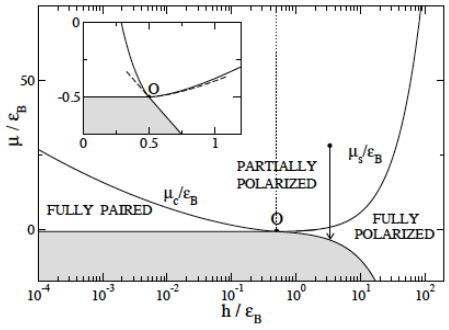

Figure 13.7: Phase diagram of one dimensional Fermi mixtures with imbalanced populations. In a parabolic trap inhomogeneous potential provides a cut through the phase diagram at constant h and changing μ, like shown with an arrow in the figure. Figure taken from [12].

constant is a product of the density of states and the interaction strength, we realize that it may be energetically favorable to keep the low density regions unpolarized and fully paired. However, this argument does not always work. When the net polarization of the system becomes large, it becomes energetically favorable to have the edges fully polarized. Such nontrivial evolution of the spatial distribution of spin polarization has been observed in experiments [7]. A more direct evidence of the FFLO state would be the observation of the condensate of Cooper pairs at finite momentum. This can be achieved by doing projection experiment into the BEC side discussed in Chapter 11. Projection experiment should convert Cooper pairs into molecules while preserving their momenta. Hence after TOF expansion of molecules one expects to see peaks of molecular distributions at finite wavevectors. Another possibility is to measure noise correlations between $p + \frac{q}{2}$ and $-p + \frac{q}{2}$ atom pairs [14]. A major difficulty to both experiments is inhomogeneous density, which makes the FFLO wavevector take different values in different parts of the trap.

13.4 Polarons

13.4.1 Variational wavefunction

In the extreme case of very low concentration of minority atoms we can describe the system as an ensemble of non-interacting polarons. The nature of polaron states is well described by the variational wavefunction proposed by Chevy[4, 3].

$$|\Psi_{\text{polaron}}\rangle = \phi_0\, c^\dagger_{\downarrow p=0}|\text{FS}\rangle + \sum_{kq} \phi_{kq} c^\dagger_{\downarrow q-k} c^\dagger_{\uparrow k} c_{\uparrow q}|\text{FS}\rangle \tag{13.7}$$

Here $c^\dagger_{\downarrow q}$ is a creation operator for the minority atom, $c^\dagger_{\uparrow q}$ is a creation operator for the majority atoms, $|\text{FS}\rangle$ is a filled Fermi sea. Note that everywhere in

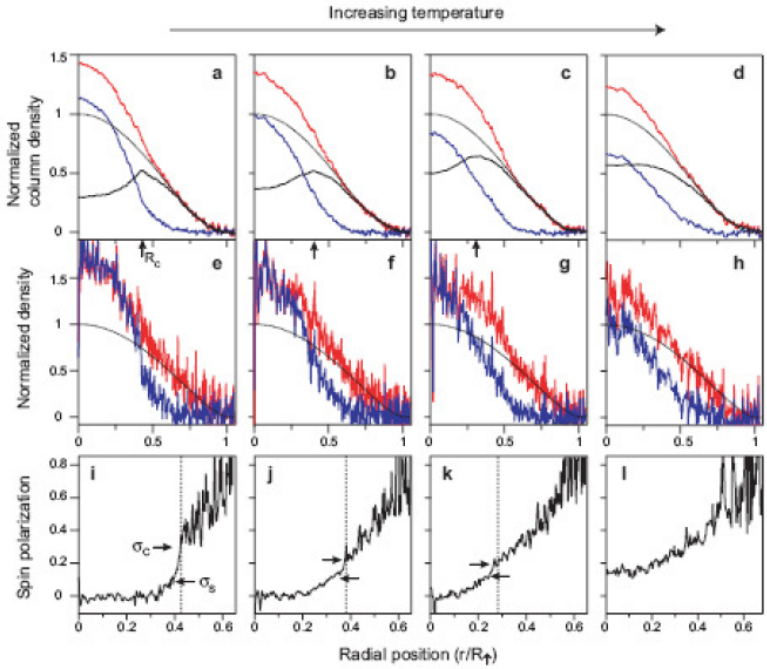

Figure 13.8: Density profiles of trapped Fermi mixtures with imbalanced populations. The first row shows columnar densities profiles, i.e. 3d densities integrated over two directions. The second and third rows show reconstructed 3D density distributions. Red line corresponds to the majority species, blue line to the minority species. In figures e)-g) there is no spin polarization in the center, indicating fully paired states. In these cases all polarization is pushed to the edges of the cloud. A jump in polarization indicates first order phase transition. Figure taken from [8].

this chapter summation over q means $q < k_F$ and summation over k means $k > k_F$. The second term in (13.7) describes particle-hole excitations created by scattering of the minority atom. It is quite remarkable that including only a single scattered p-h pair provides a good trial wavefunction. Wavefunction (13.7) was written for a polaron at zero momentum but can be trivially extended to describe polarons at finite momenta.

We again take the Hamiltonian to have contact interaction with a short distance cut-off R.

$$\mathcal{H} = \sum_{k\sigma} \epsilon_k \, c^\dagger_{k\sigma} \, c_{k\sigma} \; + \sum_{k_1+k_2=k_3+k_4} c^\dagger_{k_1\uparrow} c^\dagger_{k_2\downarrow} c_{k_3\downarrow} c_{k_4\uparrow} \tag{13.8}$$

We take expectation value of the Hamiltonian (13.8) over the polaron wavefunc-

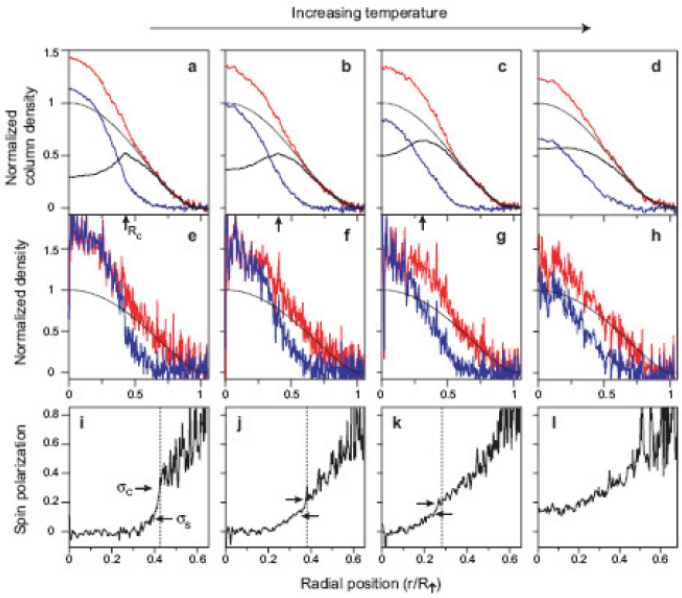

Figure 13.9: Density profiles of trapped Fermi mixtures with imbalanced populations. The first row shows columnar densities profiles, i.e. 3d densities integrated over two directions. The second and third rows show reconstructed 3D density distributions. Red line corresponds to the majority species, blue line to the minority species. In figures e)-g) there is no spin polarization in the center, indicating fully paired states. In these cases all polarization is pushed to the edges of the cloud. A jump in polarization indicates first order phase transition. Figure taken from [8].

tion (13.7)

$$\begin{aligned}
&\langle\, \Psi_{\rm polaron} \,|\, \mathcal{H} \,|\, \Psi_{\rm polaron} \,\rangle = \\
&\int \frac{d^3k}{(2\pi)^3}\,\frac{d^3q}{(2\pi)^3}\,|\phi_{kq}|^2(\epsilon_k+\epsilon_{q-k}-\epsilon_q) \;+\; V\,n\,|\phi_0|^2 \;+\; V\,n\int \frac{d^3k}{(2\pi)^3}\,\frac{d^3q}{(2\pi)^3}\,|\phi_{kq}|^2 \\
+\;& V\int \frac{d^3k}{(2\pi)^3}\,\frac{d^3k'}{(2\pi)^3}\,\frac{d^3q}{(2\pi)^3}\,\phi^*_{k'q}\,\phi_{kq} + V\int \frac{d^3k}{(2\pi)^3}\,\frac{d^3k'}{(2\pi)^3}\,\frac{d^3q}{(2\pi)^3}\,\phi^*_{kq}\,\phi_{kq'} \\
+\;& \int \frac{d^3k}{(2\pi)^3}\,\frac{d^3q}{(2\pi)^3}\,(\,\phi^*_0\phi_{kq}+\phi_0\phi^*_{kq}\,)
\end{aligned} \tag{13.9}$$

Here n is the density of majority fermions, $q < k_F$, k and $k' > k_F$. There is also UV cut-off in the k integrals at R^{-1}. We need to minimize (13.9) with respect to ϕ_0 and ϕ_{kq} with the constraint that the wavefunction is normalized. This

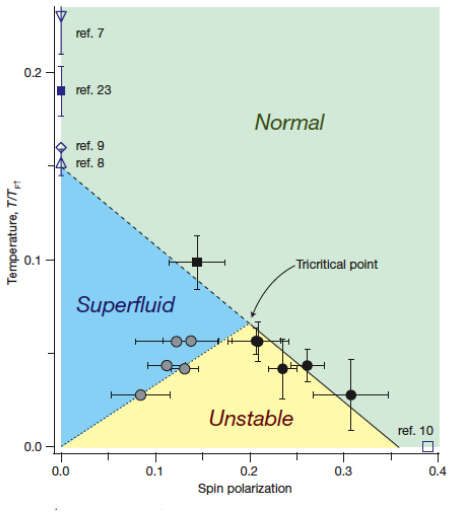

Figure 13.10: Experimentally obtained phase diagram of 3D Fermi mixtures with imbalanced populations. Figure taken from [8].

can be done by adding a Lagrange multipler

$$\frac{\delta}{\delta\phi_i^*}\left\{\langle\,\Psi_{\rm polaron}\,|\,\mathcal{H}\,|\,\Psi_{\rm polaron}\,\rangle - \lambda(\,|\phi_0|^2 + \int \frac{d^3k}{(2\pi)^3}\,\frac{d^3q}{(2\pi)^3}\,|\phi_{kq}|^2\,)\right\} = 0 \tag{13.10}$$

where ϕ_i stads for ϕ_0 and ϕ_{kq}. We have

$$V\,n\,\phi_0 \quad + \quad V\int \frac{d^3k}{(2\pi)^3}\,\frac{d^3q}{(2\pi)^3}\,\phi_{kq} - E\phi_0 = 0 \tag{13.11}$$

$$(\epsilon_k + \epsilon_{q-k} - \epsilon_q)\phi_{kq} \quad + \quad Vn\phi_{kq} + V\int \frac{d^3k'}{(2\pi)^3}\,\phi_{k'q} + V\int \frac{d^3q'}{(2\pi)^3}\,\phi_{k'q} + V\phi_0 - E\phi_{kq} = 0 \tag{13.12}$$

In writing the last equation we used the fact that lagrange multiplier becomes equal to the energy. This can be proven by multiplying (13.11) by ϕ_0^*, (13.12) by ϕ_{kq}^* and summing them, including integration ovr k and q. Before we start analyzing equations (13.11), (13.12), it is useful to recall that our strategy is to send the momentum cut-off R^{-1} to infinity, while taking the microscopic interaction V to zero, in such a way that the scattering length remains finite. Then it is easy to see that some terms in these equations vanish in the limit $R \to 0$ and can therefore be neglected from the very beginning. Simple scaling arguments require that $\phi_{kq} \sim R^{3/2}$ and $V \sim R^{3/2}$. Note that integration over q adds a factor of the order of k_F^3, while integration over k adds a factor of the order of R^{-3}. Then we can neglect the first term in (13.11) since this term is suppressed as $R^{3/2}$ with respect to other terms in this equations. Analogously

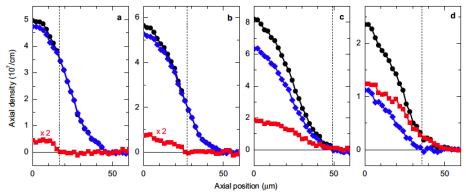

Figure 13.11: Axial density profiles of Fermi mixtures with imbalanced populations in 1d tubes [7]. Black circles correspond to species, blue diamonds to minority species, red squared to the difference of the two desnitites. For small polarizations in a) and b) the edge is fully paired. At large polarization in d) the edge is fully polarized and the minority density vanishes. Figure taken from [7].

we can neglect the second and the fourth terms in (13.12). Hence we have

$$V \int \frac{d^3k}{(2\pi)^3} \frac{d^3q}{(2\pi)^3} \phi_{kq} - E\phi_0 = 0 \quad (13.13)$$

$$(\epsilon_k + \epsilon_{q-k} - \epsilon_q)\phi_{kq} + V \int \frac{d^3k'}{(2\pi)^3} \phi_{k'q} + V\phi_0 - E\phi_{kq} = 0 \quad (13.14)$$

We can use these equations to obtain an equation for the polaron energy (see section 13.6 for details)

$$E = \int_{q<k_F} \frac{d^3q}{(2\pi)^3} \left[\frac{1}{\frac{1}{V} - \int_{k>k_F} \frac{d^3k}{(2\pi)^3} \frac{1}{E-(\epsilon_k+\epsilon_{q-k}-\epsilon_q)}} \right] \quad (13.15)$$

We use the usual approach of rewriting the bare interaction using the scattering length following equation (13.4), and obtain

$$E = \int_{q<k_F} \frac{d^3q}{(2\pi)^3} \left[\frac{1}{\frac{m}{4\pi\hbar^2 a} - \int_{k<k_F} \frac{d^3k}{(2\pi)^3} \frac{1}{2\epsilon_k} - \int_{k>k_F} \frac{d^3k}{(2\pi)^3} \left(\frac{1}{E-(\epsilon_k+\epsilon_{q-k}-\epsilon_q)} + \frac{1}{2\epsilon_k} \right)} \right] \quad (13.16)$$

When $a \to 0^-$ the denomenator is dominated by the $1/a$ term and we find

$$E \sim \frac{4\pi\hbar^2 a}{m} \int_{q<k_F} \frac{d^3q}{(2\pi)^3} = \frac{4\pi\hbar^2 a\, n}{m} \quad (13.17)$$

This is the mean-field shift. When $a \to 0^+$ we can write equation (13.16) as (this requires some work)

$$E = \int_{q<k_F} \frac{d^3q}{(2\pi)^3} \left[\frac{1}{\frac{m}{4\pi\hbar^2 a} - \frac{m}{4\pi}(-mE - \frac{q^2}{4})^{1/2}} \right] \quad (13.18)$$

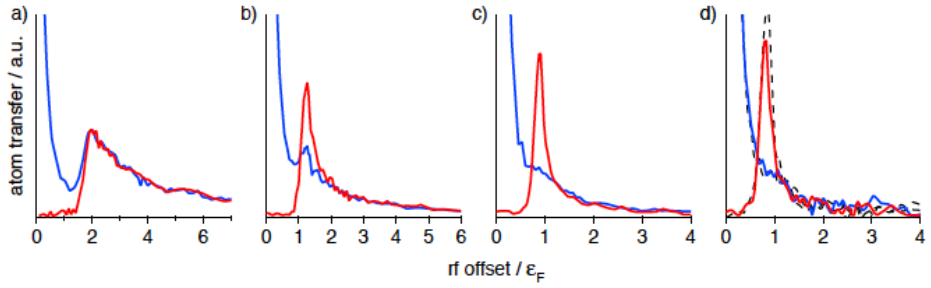

Figure 13.12: RF spectroscopy of polarons. Blue line is for the majority component, red line is for the minority component. a) is moleclar limit; b) and c) correspond to emergence of polaron; d) is at unitarity. In the case of polarons there is a distinct peak exclusively in the minority component. Figure taken from [5].

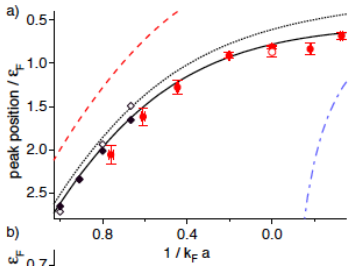

Figure 13.13: Peaks of the minority species RF spectrum as a measure of the polaron energy. Dotted line: polaron energy from the variational ansatz (13.7) obtained using equation (13.16). The solid line includes weak final state interactions. Red dashed line - energy of an isolated molecule in vacuum. Blue dash-dotted line : mean-field limit for an impurity atom. Figure taken from [5].

It is clear that in this case $E \approx -\frac{\hbar^2}{ma^2}$. At unitarity one finds $E \approx -0.3\frac{\hbar^2 k_F^2}{m}$.

The main limitation of the variational ansatz (13.7) is that it predicts polaron type states for any value of the interaction. Diagrammatic Monte-Carlo shows that there is a transition into molecular state for $1/(k_F a) > 0.9$[13] . Formation of molecules can be approximately understood as vanishing of ϕ_0 in (13.7).

13.4.2 Experimental observation of polarons

Detailed study of polarons has been done using RF spectroscopy by [5]

13.5 Appendix. Bogoliubov de Gennes equations

Previously we discussed fermionic systems with attractive interactions that are homogenous. We now consider the more general case when fermions can experience an arbitrary external or self-constently generated potential. We take

$$\begin{aligned} \mathcal{H} &= \mathcal{H}_0 + \mathcal{H}_1 \\ \mathcal{H}_0 &= \int dr \sum_\sigma \Psi^\dagger_\sigma(r)[\,\frac{p^2}{2m} + U(r) - \mu_\sigma\,]\,\Psi_\sigma(r) \\ \mathcal{H}_1 &= +V\int dr\,\Psi^\dagger_\uparrow(r)\,\Psi^\dagger_\downarrow(r)\,\Psi_\downarrow(r)\,\Psi_\uparrow(r) \end{aligned} \tag{13.19}$$

We replace the interaction term by the local one-body potential

$$\mathcal{H}_{1\text{eff}} = \int dr\,[\,-\Delta^*(r)\,\Psi_\downarrow(r)\,\Psi_\uparrow(r) \;-\; -\Delta(r)\,\Psi^\dagger_\uparrow(r)\,\Psi^\dagger_\downarrow(r) \;-\; \frac{|\Delta|^2}{V}] \tag{13.20}$$

Hamiltonian $\mathcal{H}_{\text{eff}} = \mathcal{H}_0 + \mathcal{H}_{1\text{eff}}$ can be diagonalized by the generalized Bogoliubov transformation

$$\begin{aligned} \Psi_\uparrow(r) &= \sum_n [u_n(r)\gamma_{n\uparrow} + v^*_n(r)\gamma^\dagger_{n\downarrow}\,] \\ \Psi^\dagger_\downarrow(r) &= \sum_n [-v_n(r)\gamma_{n\uparrow} + u^*_n(r)\gamma^\dagger_{n\downarrow}\,] \end{aligned} \tag{13.21}$$

We need to to find $u_n(r)$, $v_n(r)$ such that $\{\,\gamma_{n\sigma}, \gamma^\dagger_{n'\sigma'}\,\} = \delta_{nn'}\,\delta_{\sigma\sigma'}$ and $\mathcal{H}_{\text{eff}} = \sum_{n\sigma} E_{n\sigma}\gamma^\dagger_{n\sigma}\gamma_{n\sigma}$. To find $u_n(r)$ and $v_n(r)$ we observe that $[\mathcal{H}_{\text{eff}}, \gamma^\dagger_{n\sigma}] = E_{n\sigma}\gamma^\dagger_{n\sigma}$ and $[\mathcal{H}_{\text{eff}}, \gamma_{n\sigma}] = -E_{n\sigma}\gamma_{n\sigma}$. We can now calculate

$$\begin{aligned} [\Psi_\uparrow(r), \mathcal{H}_{\text{eff}}] &= \hat{\mathcal{H}}_0\Psi_\uparrow(r) + \Delta(r)\Psi^\dagger_\downarrow(r) \\ &= \sum_n [E_{n\uparrow}u_n(r)\gamma_{n\uparrow} \;-\; E_{n\downarrow}v^*_n(r)\gamma^\dagger_{n\downarrow}\,] \end{aligned} \tag{13.22}$$

We compare the $\gamma_{n\uparrow}$ and $\gamma^\dagger_{n\downarrow}$ parts of the last equation and find

$$E_{n\sigma} = E_n - \sigma h \tag{13.23}$$

and

$$\begin{pmatrix} -\frac{\hbar^2\nabla^2}{2m} - \mu & \Delta(r) \\ \Delta^*(r) & \frac{\hbar^2\nabla^2}{2m} + \mu \end{pmatrix} \begin{pmatrix} u_n(r) \\ v_n(r) \end{pmatrix} = E_n \begin{pmatrix} u_n(r) \\ v_n(r) \end{pmatrix} \tag{13.24}$$

We find the free energy

$$F = \int d^3r\,[\sum_n(-2E_n|v_n(r)|^2 + \frac{|\Delta(r)|^2}{2\epsilon_n}) - \frac{m}{4\pi\hbar^2 a}\,|\Delta(r)|^2\,] + \sum_n (E_n - h)f(E_n - h) \tag{13.25}$$

In the last equation the interaction strength V was expressed in terms of the scattering length a as in (13.4). This lead to the appearance of the $\sum_n \frac{|\Delta(r)|^2}{2\epsilon_n}$ term, with ϵ_n being normal state energies, which in principle should be different eigenstates. The last term in (13.25) arises from the occupation of states with $E_n - h < 0$. We are interested in domain wall energy for a given μ, h, and a. This is calculated as the energy difference between a state with a single planar domain wall and the uniform state. For many practical purposes it is sufficient to take a variational ansatz

$$\Delta(z) = \Delta_0 tanh\left((2m\mu)^{1/2} \frac{z}{\kappa} \right) \tag{13.26}$$

Parameter κ is variational. Analysis of Yoshida and Yip [15] produces the phase diagram shown in figure 13.5

13.6 Appendix. Techincal details in the derivation of the polaron energy

We denote

$$\chi(q) = \phi_0 + \int \frac{d^3k'}{(2\pi)^3} \phi_{k'q} \tag{13.27}$$

Then from equation (13.14) we have

$$\phi_{kq} = \frac{V\,\chi(q)}{E - (\epsilon_k + \epsilon_{q-k} - \epsilon_q)} \tag{13.28}$$

We can now write

$$\phi_0 = \chi(q) - \int \frac{d^3k}{(2\pi)^3} \phi_{kq} = \chi(q) \left[1 - V \int \frac{d^3k}{(2\pi)^3} \frac{1}{E - (\epsilon_k + \epsilon_{q-k} - \epsilon_q)} \right] \tag{13.29}$$

Form equation (13.13) we find

$$\frac{E}{V}\phi_0 = \int \frac{d^3k}{(2\pi)^3} \frac{d^3q}{(2\pi)^3} \phi_{kq} = \int \frac{d^3q}{(2\pi)^3} [\,\chi(q) - \phi_0\,] \tag{13.30}$$

In writing the last equation we used (13.27). We recall that integration over q goes only up to k_F, then quation (13.30) can be written as

$$\phi_0 \left(\frac{E}{V} + \frac{4\pi k_f^3}{3\,(2\pi)^3} \right) = \int \frac{d^3q}{(2\pi)^3} \chi(q) \tag{13.31}$$

Since $V \sim R^{3/2}$ and $R^{-1} >> k_F$ we can neglect the second term in the left hand side of (13.31). Hence we obtain

$$\frac{E}{V}\,\phi_0 = \int \frac{d^3q}{(2\pi)^3} \chi(q) \tag{13.32}$$

Combining equations (13.29) and (13.32) we have

$$\chi(q) = \frac{\frac{1}{E}\int \frac{d^3q}{(2\pi)^3}\,\chi(q)}{\frac{1}{V} - \int \frac{d^3k}{(2\pi)^3}\,\frac{1}{E-(\epsilon_k+\epsilon_{q-k}-\epsilon_q)}} \tag{13.33}$$

Equation (13.15) for the polaron energy is then obvious.

13.7 Problems to Chapter 13

Problem 1.

Consider a Bose-Fermi mixture described by the Hamiltonian

$$\mathcal{H} = \sum_k \epsilon_{\mathrm{f}\,k} f_k^\dagger f_k + \sum_k \epsilon_{\mathrm{b}\,k} b_k^\dagger b_k + \frac{U_{bb}}{2}\int dr\, n_b(r) n_b(r) + U_{bf}\int dr\, n_b(r) n_f(r) \tag{13.34}$$

Here $b^\dagger$ and $f^\dagger$ are creation operators for bosons and fermions respectively, n_b is the density of bosons, and n_f is the density of fermions. In the mean field approximation the energy of the system can be taken as

$$E_{MF} = \frac{3}{5}E_F n_f + \frac{U_{bb}}{2}n_b^2 + U_{bf} n_b n_f \tag{13.35}$$

Here E_F is the Fermi energy of fermions (which is also density dependent!) Use this expression of E_{MF} to derive the immiscibility condition for Bose-Fermi mixtures. Discuss implications of this result for the phase diagram of fermionic paired systems with spin imbalance on the BEC side.

Bibliography

[1] Mark Alford, Jeffrey A. Bowers, and Krishna Rajagopal. Crystalline color superconductivity. *Phys. Rev. D*, 63(7):074016, Mar 2001.

[2] Mark G. Alford, Andreas Schmitt, Krishna Rajagopal, and Thomas Schäfer. Color superconductivity in dense quark matter. *Rev. Mod. Phys.*, 80(4):1455–1515, Nov 2008.

[3] F. Chevy.

[4] F. Chevy. Universal phase diagram of a strongly interacting fermi gas with unbalanced spin populations. *Phys. Rev. A*, 74(6):063628, Dec 2006.

[5] A.Schirotzek et al. *Phys. Rev. Lett.*, 102:230402, 2009.

[6] M. Parish et al. *Nature Physics*, 3:124, 2007.

[7] Y. Liao et al. *Nature*, 467:567, 2010.

[8] Y. Shin et al. *Nature*, 451:689, 2008.

[9] Peter Fulde and Richard A. Ferrell. Superconductivity in a strong spin-exchange field. *Phys. Rev.*, 135(3A):A550–A563, Aug 1964.

[10] A.I. Larkin and Y.N. Ovchinnikov. *Sov. Phys. JETP*, 20:762, 1965.

[11] Y. Matsuda and H. Shimahara. *J. Phys. Soc. Jpn.*, 76:51005, 2007.

[12] G. Orso. *Phys. rev. Lett.*, 98:70402, 2007.

[13] N. Prokof'ev and B. Svistunov. *Phys. Rev. B*, 77:20408(R), 2008.

[14] K. Yang. *Phys. Rev. Lett.*, 95:218903, 2005.

[15] Yoshida and Yip. *Phys. Rev. A*, 75:63601, 2007.